New cathode materials for rechargeable Mg batteries: fast Mg ion transport and reversible copper extrusion in $Cu_yMo_6S_8$ compounds†

A. Mitelman, M. D. Levi,* E. Lancry, E. Levi and D. Aurbach

Received (in Cambridge, UK) 13th July 2007, Accepted 29th August 2007
First published as an Advance Article on the web 5th September 2007
DOI: 10.1039/b710743a

We report on a discovery of fast cathode materials, ternary Chevrel phases (CPs), $Cu_yMo_6S_8$, for rechargeable magnesium batteries; the related electrochemical process displays a unique coupling between reversible Mg insertion, and Cu extrusion/reinsertion; this coupling results in an entirely new intercalation mechanism which combines the total chemical reversibility of the electrochemical reaction of $Mg_xCu_yMo_6S_8$ with irreversibility of its separate stages once Cu extrusion stage is reached (in $Mg_xCu_yMo_6S_8$: $0.5x + y > 4$).

Chevrel phases (CPs), $M_xMo_6T_8$ (M = metal, T = S, Se, Te) are a unique class of host materials which can reversibly intercalate a variety of cations (including multivalent ones).[1] This is due to their specific crystallographic structure consisting of the pseudo-cubic cavities between the Mo_6T_8 blocks (*i.e.* octahedral clusters of Mo atoms inside cubic anionic framework). The structure, which contains Mo_6 clusters with variable valence, a flexible anionic framework, multidirectional diffusion paths and several types of cavities for inserted cations, enables the accommodation of intercalated cations of different sizes, while the Mo_6 clusters can adopt simultaneously charge injection of up to four electrons. Special interest is aroused by ternary CPs which are able to insert two different cations. In an early report[2] Jui, McKinnon and Dahn furnished conclusive evidence that ternary CPs are capable of Li^+ insertion in organic electrolyte solutions. Studying the phase diagram of $Li_xCu_yMo_6S_8$, they noted that this insertion is coupled with segregation (clustering) of the Cu^+ ions in the CPs structure, and, finally, at a discharge level corresponding to $x + y > 4$, Cu extrusion takes place. In this report, no reinsertion of Cu^+ ions into the host structure was observed upon charge. In contrast, characterizing two new ternary hosts, $Cu_{1.1}V_4O_{11}$[3] and $Cu_{2.33}V_4O_{11}$,[4] that exhibit Cu extrusion upon Li^+ intercalation, Tarascon and co-workers presented convincing evidence of a partial Cu^+ reinsertion into the former host, and proved a peculiar phenomenon of amorphization/recrystallization of $Cu_{2.33}V_4O_{11}$ upon its charge and discharge.

Recently, a new concept of rechargeable Mg batteries was proposed, in which binary Mo_6S_8 cathodes, Mg metal anodes, and novel ethereal solutions containing $(R_2Mg)_n(AlCl_{3-n}R'_n)_m$ complexes (R, R′ = alkyl groups) were used.[5] This system was shown to be repeatedly cycled in a particularly reversible manner. Here we show that the utilization of these solutions (which neither dissolve Cu salts nor react with Cu metal) with $Cu_yMo_6S_8$ electrode improves substantially the battery's performance. It does so by imparting to the charge–discharge process the unusually high efficiency (100%) of the electrochemical reaction due to Cu extrusion at the end of discharge, and full Cu reinsertion into the ternary host structure upon Mg^{2+} deinsertion (charge). This process is presented and elucidated in comparison with the common mechanism of Mg^{2+} insertion into the binary, metal-free Mo_6S_8[6] (the related structural data will appear elsewhere).[7]

For the electrochemical measurements we used composite powder electrodes comprising 80% $CuMo_6S_8$ (synthesized as reported elsewhere,[5] see also ESI†), 10% PVdF binder and 10% conductive carbon black additive. The experiments were performed in three-electrode flooded cells with Mg counter and reference electrodes, in a glove box (VAC Inc.) at room temperature. These conditions are practically identical to those used for the studies of the binary Mo_6S_8 electrodes.[5,8] The preparation procedures of the ethereal solutions of $(R_2Mg)_n(AlCl_{3-n}R'_n)_m$ complexes were also reported earlier.[9]

Fig. 1 shows a typical, steady state, slow scan rate (at 5 μV s^{-1}) cyclic voltammetry (SSCV) response of Mg^{2+} insertion into

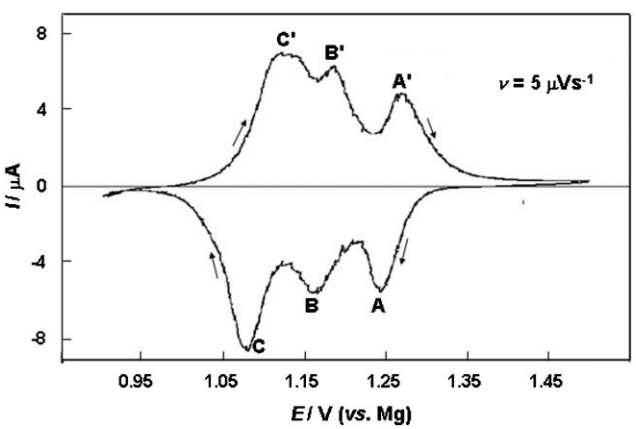

Fig. 1 SSCV curve for the Mg insertion/deinsertion into/from $CuMo_6S_8$ composite electrode (~1 mg active mass) measured at 5 μV s^{-1} in a narrow potential range.

Department of Chemistry, Bar-Ilan University, Ramat-Gan 52900, Israel. E-mail: levimi@mail.biu.ac.il; Fax: (972)-3-7384053; Tel: (972)-3-5318832

† Electronic supplementary information (ESI) available: Brief description of the synthesis of the precursor. Fig. 1S: (a) Rietveld analysis of the product of chemical Mg intercalation into $Cu_yMo_6S_8$ (the air-stored sample); (b) HRTEM micrograph for the fully discharged product of the composition $Cu^0 + Mg_2Mo_6S_8$; (c) FFT analysis of the marked area in panel (b). Fig. 2S: Cyclic voltammetry for the $Cu_yMo_6S_8$ electrodes containing different initial amount of copper. Scheme 1S: Stoichiometries of the cathodic and anodic reactions obtained by combined integration of the cyclic voltammetry curve in Fig. 2 and the curves obtained by intermittent reversal linear voltammetry. Fig. 3S: Cycling ability of a coin-type cell with $CuMo_6S_8$ cathode and Mg anode measured at C/6 rate at 30 °C. See DOI: 10.1039/b710743a

$CuMo_6S_8$ in a narrow potential range, from 1.50 to 0.95 V *vs.* Mg. Under these conditions, the ion-insertion process is fully *chemically reversible for each* of the three consecutive steps (see redox-peaks A/A′, B/B′ and C/C′ in Fig. 1). Lowering the cathodic vertex potential to 0.5 V (*i.e.* increasing the Mg^{2+} insertion level), added a new intercalation stage, denoted as D (See Fig. 2). In the following positive potential scan a new set of five peaks, marked from I to V in Fig. 2 were revealed. These peaks differed from the related anodic peaks A′, B′ and C′ in Fig. 1, both in potentials and heights

This experiment shows that as $CuMo_6S_8$ is driven to low cathodic potential, the system is not chemically reversible *for each* separate step of the insertion (deinsertion) process. Nevertheless, the integration of the CV curve in Fig. 2 proves that the entire insertion-deinsertion process is still highly *chemically reversible*: the total Faradaic efficiency for the ternary CP cycled in the wider potential range was close to 100%, independent of the cycle number. The peculiar combination of chemical irreversibilities of separate stages with the full reversibility of the Mg insertion/deinsertion and Cu extrusion/reinsertion conveys two new features to the known intercalation reactions: (i) the Mg^{2+} ion transportation in the ternary CP improves in comparison to the binary CP, so that the effect of Mg^{2+} trapping is completely eliminated (compare with 25% charge loss for the binary Mo_6S_8 electrode at room temperature);[8] (ii) the last step of Mg insertion (*i.e.* peak D in Fig. 2) relates to Cu extrusion from the CPs' crystal structure, which was confirmed by Rietveld analysis of the fully discharged (reduced) product (see ESI,† Fig. 1S), and by fast Fourier Transform (FFT) analysis of the HRTEM image focused on the metallic copper lattice (ESI,† Fig. 1S(b) and (c)). In addition, varying the Cu content (y) in the initial $Cu_yMo_6S_8$, in the sequence 0, 0.2, 0.4 and 1.0, we noted that the integrated area under peak D is linearly proportional to y (see ESI,† Fig. 2S). The structural analysis[7] showed also that the set of anodic peaks from I to V in Fig. 2 reflects a peculiar coupling of Mg deinsertion with Cu reinsertion into the ternary host, which occurs in five separate steps.

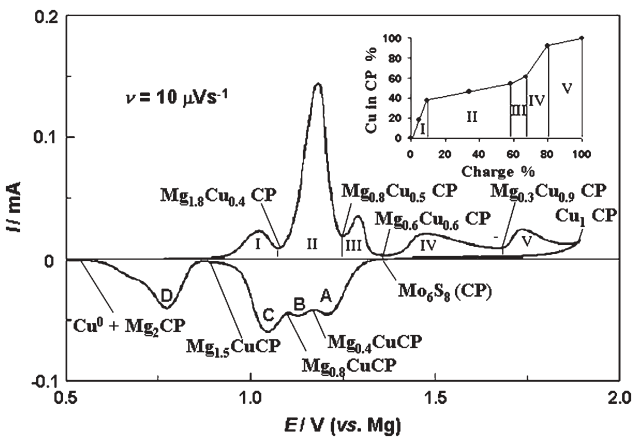

Fig. 2 SSCV curve for the Mg insertion/deinsertion into/from $CuMo_6S_8$ composite electrode (~5 mg active mass) measured at 10 μV s^{-1}. Phase compositions are indicated. Inset shows the percentage of reinserted Cu as a function of the charge level obtained by *intermittent reversal linear voltammetry*.

In order to calculate the amount of the reinserted Cu in each step, we ran *intermittent reversal linear voltammetry* as follows: following Mg^{2+} deinsertion, as the potentials of pure phases were attained (*i.e.* at the saddle points in the anodic part of the curve in Fig. 2, marked by the vertical lines), the scan was reversed down to 0.5 V, and the area under the peak related to Cu extrusion (*i.e.* peak D in Fig. 2) was assigned to the amount of Cu^+ reinserted at the different levels of Mg^{2+} deinsertion (during charging). The percentage of the reinserted Cu^+ as a function of the Mg^{2+} deinsertion level is shown in the inset in Fig. 2. These data, together with the coulometric data obtained from integration of the SSCV curve in Fig. 2, were used to determine the average stoichiometries of the phases formed in the course of Mg^{2+} deinsertion from this system (coupled with Cu^+ reinsertion), as indicated in Fig. 2. The entire set of cathodic and anodic reactions of these systems is presented in the ESI† (Scheme 1S, eqn (1)–(9)).

Fig. 3(a) and (b) describe schematically the mechanisms of Mg^{2+} insertion and deinsertion, respectively. Here the cumulative charge of each CV peak is presented as number of electrons (up to four electrons per Mo_6S_8 unit) and plotted as a function of the electrode's potential (the dashed lines). The cathodic and anodic

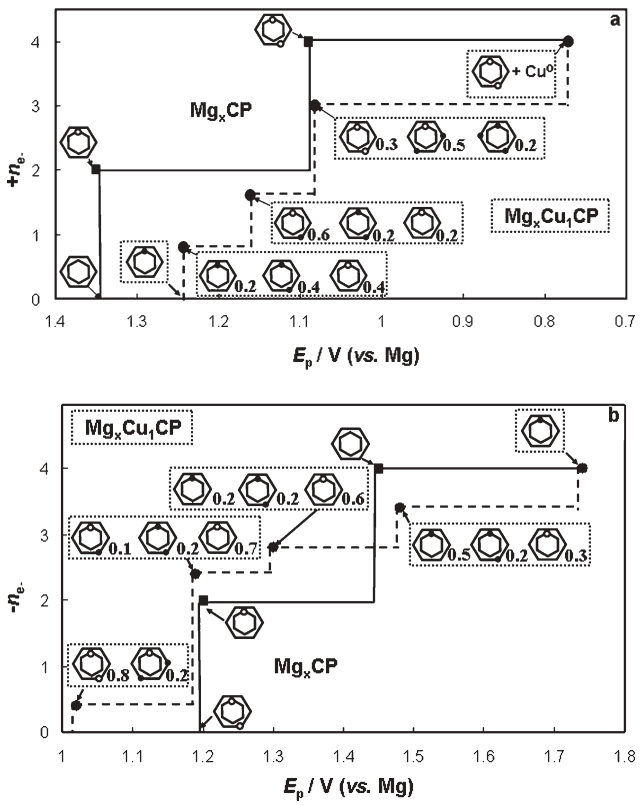

Fig. 3 The number of electrons transferred per single Mo_6S_8 unit as a function of the cathodic (a) and anodic (b) SSCV peak potentials (upon discharge and charge, respectively). The potentials marked by broken and solid lines relate to the ternary and binary CPs ($CuMo_6S_8$ and Mo_6S_8), respectively. They are associated with structural fragments (site assemblies in the dotted frames for the $CuMo_6S_8$ host and without dotted frames for the Mo_6S_8 host) in the intercalation compounds characterizing the arrangement of Mg^{2+} and Cu^+ cations (the open and solid circles, respectively) on the 12 possible sites (6 sites per ring). The numbers near the fragments are their fractions (for more details see ref. 7). Note reversed potential scales here are consistent with reversed directions of charge flow.

SSCV peak potentials serve here as a measure of the difference in the potential energies involved in the corresponding phase transitions. For comparison, the solid lines in Fig. 3(a) and (b) relate to Mg^{2+} insertion/deinsertion into/from the binary Mo_6S_8 host. In the latter case we neglected a partial Mg trapping, always occurring in the binary Mo_6S_8 at room temperature, which considerably affects the potential of the first differential capacitance peak appearing at the beginning of discharge. Fortunately, the effect of trapping is eliminated at higher temperatures, so that the data for the Mo_6S_8 host refer to 60 °C.[8]

The various phases formed in the course of the two processes at the relevant potentials contain certain combinations of structural fragments (site assemblies) (The framed and unframed site assemblies marked in Fig. 3(a) and (b) pertain to the ternary and binary hosts, respectively; see also the captions). The fragments illustrate the arrangement of Mg^{2+} and Cu^{+} cations (the open and solid circles, respectively) within the 12 possible sites (6 sites per ring, the inner and outer one). For the binary host, two stoichiometric $MgMo_6S_8$ and $Mg_2Mo_6S_8$ phases are involved in the two sequential phase transitions as x increases from 0 to 2 (see the solid lines in Fig. 3(a) and (b) and the related sites occupied by Mg^{2+} cations). In contrast, the electrochemical processes for the ternary host, reflected by the SSCV curve of Fig. 2, produce mixed phases, $Mg_xCu_yMo_6S_8$, which differ by the amount of Cu^{+} and Mg^{2+} cations occupying the various sites in the inner and outer rings, as shown in Fig. 3(a) and (b). The structural details of these phases are discussed thoroughly elsewhere.[7]

Fig. 3(b) shows very clearly how the insertion of the Mg^{2+} ions into the inner sites of the ternary $CuMo_6S_8$ host, splits a single energetic level existing in the pristine material into two sublevels. The latter are related not only to Mg^{2+} insertion, but also to the concomitant regrouping of the Cu^{+} ions, and the formation of the Mg–Cu assemblies. It is remarkable that Mg^{2+} occupation in the outer rings occurs at approximately the same potential, around 1.1 V, for the ternary and binary CPs (Fig. 3(a)). In the former case, this insertion causes further Cu^{+}-ion segregation with the formation of Cu–Cu–Cu and Cu–Cu–Mg assemblies. At lower potentials (peak D), Cu is extruded from the last two assemblies forming metallic Cu and purely stoichiometric $Mg_2Mo_6S_8$ phase (Fig. 3).

Similar considerations can be applied to interpret the formation of the different non-stoichiometric phases during Mg^{2+} deinsertion from the Cu–$Mg_2Mo_6S_8$ mixture (see Fig. 3(b)). However, the number of the phases formed, and their compositions, are different. From the potentials of the peaks D and I in Fig. 2 one clearly realizes that the anodic dissolution of Cu^0 is thermodynamically feasible *well before* the thermodynamic potential of the first electrochemical removal of Mg^{2+} ions from the outer rings (about 1.2 V, see Fig. 3(b)). The unique and quite unusual feature of the deinsertion mechanism is due to the fact that Cu cannot anodically dissolve at this potential into the bulk of the ethereal solutions used. Hence, Cu^{+} ions are reinserted into the CPs sequentially, in five separate steps. It is the coupling of Cu reinsertion with the Mg deinsertion that leads to the peculiarity of the resulting charging process, as reflected by the anodic voltammetric response (five separate peaks, Fig. 2).

Processes as those indicated herein have never been reported before for any ternary intercalation compound. The most important new features discovered are summarized below. (i) The first Mg deinsertion process (peak I in Fig. 1) is pure exchange between Mg^{2+} and $2Cu^{+}$: the passing charge is associated with partial ionization of Cu^0 only. (ii) Similar structural fragments (Cu–Mg ionic assemblies) are formed during charge and discharge. Note, however, that the Cu-rich phase, containing the assembly of three Cu^{+} ions, is formed during discharge process only (compare the cationic assemblies in Fig. 3(a) and (b)). (iii) The thermodynamic availability of Cu^{+} ions (due to oxidation of Cu^0 at a relatively low potential) leads to a larger number, and different compositions of the phases that are formed during the charging process as compared to that for the discharge. This causes the appearance of chemical irreversibility of *each* stage of Mg^{2+} deinsertion, once a deep discharge level of the electrode is reached.

It should be noted that $CuMo_6S_8$ can serve as a fast cathode material for rechargeable Mg batteries. Prototype Mg batteries containing $CuMo_6S_8$ cathodes could be cycled hundreds of times with no charge trapping limitations and negligible charge loss (see ESI,† Fig. 3S). Since the theoretical capacity of this ternary phase is only slightly lower than that of the binary phase (114 *vs.* 122 mA h g^{-1}, respectively), it appears that in terms of rates and practical capacities (100 *vs.* 90 mA h g^{-1}, respectively, after 100 cycles), $CuMo_6S_8$ is superior to Mo_6S_8 at room temperature.

Partial supports for this work were obtained by GIF (German-Israel foundation) and the BSF (Israel-USA binational foundation).

Notes and references

1 K. Yvon, *Curr. Top. Mater. Sci.*, 1979, **3**, 53.
2 C. C. H. Jui, W. R. McKinnon and J. R. Dahn, *Phys. Rev. Lett.*, 1985, **54**, 1432.
3 M. Morcrette, P. Martin, P. Rozier, H. Vezin, F. Chevallier, L. Laffont, P. Poizot and J.-M. Tarascon, *Chem. Mater.*, 2005, **17**, 418.
4 M. Morcrette, P. Rozier, L. Dupont, E. Mugnier, L. Sannier, J. Galy and J. M. Tarascon, *Nat. Mater.*, 2003, **2**, 755.
5 D. Aurbach, Z. Lu, A. Schechter, Y. Gofer, H. Gizbar, R. Turgeman, Y. Cohen, M. Moskovich and E. Levi, *Nature*, 2000, **407**, 724.
6 E. Levi, E. Lancry, A. Mitelman, D. Aurbach, G. Ceder, D. Morgan and O. Isnard, *Chem. Mater.*, 2006, **18**, 5492.
7 E. Levi, A. Mitelman, D. Aurbach and M. Brunelli, *Chem. Mater.*, 2007, in press.
8 M. D. Levi, E. Lancry, H. Gizbar, Y. Gofer, E. Levi and D. Aurbach, *Electrochim. Acta*, 2004, **49**, 3201; M. D. Levi, H. Gizbar, E. Lancry, Y. Gofer, E. Levi and D. Aurbach, *J. Electroanal. Chem.*, 2004, **569**, 211.
9 H. Gizbar, Y. Vestfrid, O. Chusid, Y. Gofer, H. E. Gottlieb, V. Marks and D. Aurbach, *Organometallics*, 2004, **23**, 3826.

